MULTISCALE MODELING OF FLUCTUATIONS IN STOCHASTIC ELLIPTIC PDE MODELS OF NANOSENSORS

CLEMENS HEITZINGER* AND CHRISTIAN RINGHOFER†

Abstract. In this work, the multiscale problem of modeling fluctuations in boundary layers in stochastic elliptic partial differential equations is solved by homogenization. A homogenized equation for the covariance of the solution of stochastic elliptic PDEs is derived. In addition to the homogenized equation, a rate for the covariance and variance as the cell size tends to zero is given. For the homogenized problem, an existence and uniqueness result and further properties are shown. The multiscale problem stems from the modeling of the electrostatics in nanoscale field-effect sensors, where the fluctuations arise from random charge concentrations in the cells of a boundary layer. Finally, numerical results and a numerical verification are presented.

Key words. Stochastic elliptic partial differential equation, multiscale problem, homogenization, limiting problem, rate, field-effect sensor, nanowire, BioFET.

Subject classifications. 35B27 Homogenization; equations in media with periodic structure,
35J05 Laplacian operator, reduced wave equation (Helmholtz equation), Poisson equation,
35Q92 PDEs in connection with biology and other natural sciences,
62P30 Applications in engineering and industry,
82D80 Nanostructures and nanoparticles,
92C50 Medical applications (general).

1. Introduction

A motivation for the present study of stochastic elliptic PDEs is to provide the quantitative understanding of field-effect nanowire sensors. Elliptic equations, such as the Poisson equation and the linearized Poisson-Boltzmann equation, are the basic equations for their electrostatics, and the stochastic equations considered here make it possible to quantify fluctuations and noise in nanostructures. A multiscale problem is inherent in these nanoscale structures and therefore homogenization is used.

To see where the homogenization problem arises, we introduce the physical problem first. Recently, nanoscale field-effect biosensors [30, 31, 33, 36] and gas sensors [22, 25, 29, 34, 37] have been demonstrated experimentally. A schematic diagram of such a sensor structure is shown in Fig. 1.1. The length scale of the molecules is in the Angstrom or nanometer range, whereas the length of the nanowire is in the micrometer range. This naturally gives rise to a multiscale problem [19, 20], since it is not possible to resolve both the boundary layer and the whole simulation domain using a single numerical grid.

This simulation problem also gives rise to a stochastic problem, since binding and unbinding events (in the case of biosensors), chemical reactions (in the case of gas sensors), and other stochastic processes occur in the boundary layer. Additionally, the movement of the molecules in the boundary layer can be modeled by calculating their electrostatic free energy and by using a Boltzmann distribution [18]. These effects imply that the charge concentrations in the boundary layer should be modeled by random variables.

*Department of Applied Mathematics and Theoretical Physics (DAMTP), University of Cambridge, Cambridge CB3 0WA, UK; Department of Mathematics, University of Vienna, A–1090 Vienna, Austria; AIT Austrian Institute of Technology, A–1220 Vienna, Austria. C.Heitzinger@damtp.cam.ac.uk.

†Department of Mathematics, Arizona State University, Tempe, AZ 85287, USA. Ringhofer@asu.edu.

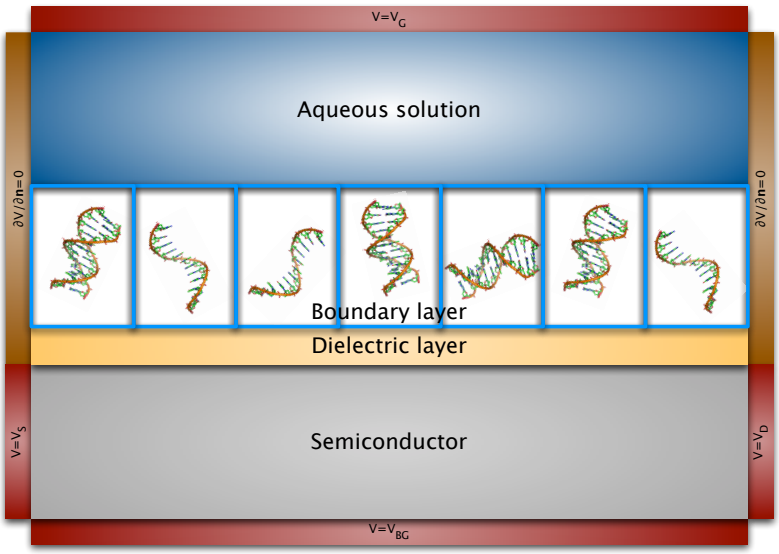

FIG. 1.1. *Schematic diagram of a typical structure considered in this work. A nanowire field-effect sensor consists of a semiconductor nanowire with two contacts at the left and at the right, a boundary layer split into cells containing random charge distributions due to biomolecules or gas molecules, and a bulk liquid or a gas atmosphere. In a DNA sensor, shown here, the immobilized probe molecules are single-stranded DNA and the target molecules are the complementary strands. After hybridization of the two strands at the sensor surface to form double-stranded DNA, the charge distribution in the biofunctionalized boundary layer is changed and hence it modulates the conductance of the semiconductor transducer. The conductance is measured between the source and drain contacts on the left and on the right.*

In previous work, we used deterministic PDE models and solved the multiscale problem for the deterministic Poisson equation $-\nabla\cdot(A\nabla u_\epsilon)=\rho_\epsilon$ with a boundary layer in [19]. Homogenization made it possible to replace the fast varying charge concentration ρ_ϵ in the boundary layer by two interface conditions for the electrostatic potential and field. The interface conditions are essentially determined by the surface-charge density and the dipole-moment density of the boundary layer.

Based on this homogenization result [19], we have shown existence and local uniqueness for a self-consistent model of field-effect sensors [8], we have developed a parallel 3d simulator for field-effect sensors [9], and we have performed realistic simulations in order to elucidate the influence of design parameters and to optimize the devices [10–13, 28].

In this work, we consider the stochastic Poisson equation

$$-\nabla\cdot\big(A(x)\nabla u_\epsilon(x,\omega)\big)=\rho(x,\frac{x}{\epsilon},\omega)$$

and generalizations thereof [2, 24, 27]. Here ω is a random variable and $\epsilon\ll 1$ is the ratio of the size of a cell in the boundary layer to the size of the simulation domain. The ultimate goal in realistic simulations, when the model equation is a stochastic PDE, is to calculate the ratio

$$\frac{Eu}{\sqrt{\operatorname{var}u}},$$

where u is the solution of the stochastic PDE and E and var are the expectation and variance operators with respect to ω, respectively. This ratio of expectation and standard deviation is a dimensionless quantity and it is often called the signal-to-noise ratio. In engineering applications such as field-effect sensors, the stochastic PDE is the stochastic linearized Poisson-Boltzmann equation and the signal-to-noise is to be maximized [18].

The main result of this work given in §3 is a deterministic, homogenized equation for the covariance of u. This equation immediately yields a way to calculate the variance as the diagonal and hence the signal-to-noise ratio. We also obtain a rate for the covariance as $\epsilon \to 0+$ as a corollary. The rate has implications for the design of field-effects sensors, since it allows to calculate noise levels.

Rigorous analysis for related problem was presented, e.g., in [5–7]. Here, the emphasis is on the presence of a boundary layer and the derivation of effective equations.

This paper is organized as follows. In §2, the stochastic Poisson-type model equations are introduced. In §3, the homogenization problem is defined and solved. The main result is the limiting equation for the covariance after homogenization; a corollary is given and some important properties of the limiting equations are shown. In §4, a discretization and numerical results are presented. Finally, §5 concludes the paper.

2. The model equations

We consider linear stochastic PDEs of the form

$$Lu(x,\omega) = \rho(x,\omega) \tag{2.1}$$

on a domain $U \subset \mathbb{R}^d$, where x is the spatial variable, ω is a random variable defined on the probability space (Ω, Σ, P), ρ is a given function, u is the unknown, and L is a linear differential operator with respect to x. An important special case is the Poisson-Boltzmann equation

$$-\nabla \cdot \big(A(x)\nabla u(x)\big) = \rho_i(x) + \rho_f(x), \tag{2.2a}$$

$$\rho_f(x) := \sum_{j\in I} z_j c_j(x) q \exp\big(-z_j q(u(x)-\phi_F)/(k_B T)\big), \tag{2.2b}$$

where A is the permittivity, u is the electrostatic potential, ρ_i is the concentration of immobile charges, and ρ_f is the concentration of free charges according to a Boltzmann distribution. I is the set of charge species (ions in liquids or electrons and holes in semiconductors), $z_j \in \mathbb{Z}$ is the valence of species j, c_j is the bulk concentration of species j, q is the elementary (proton) charge, ϕ_F is the Fermi level, k_B is the Boltzmann constant, and T is the temperature. Here the bulk concentration depends on the position x meaning that only certain sub-domains are accessible by the free charges. For physical systems such as 1:1 electrolytes (containing one species of cations and one of anions) and positive and negative charge carriers in semiconductors, we set $I := \{-1,+1\}$ and $z_j := j$ and we assume $c_{-1}(x) = c_1(x) =: c(x)$. This yields

$$\rho_f(x) = \sum_{j\in\{-1,+1\}} j c(x) q \exp\big(-jq(u(x)-\phi_F)/(k_B T)\big) = -2c(x) q \sinh\frac{q(u-\phi_F)}{k_B T}. \tag{2.3}$$

It is well-known that the following result holds for the semilinear Poisson-Boltzmann equation (2.2).

PROPOSITION 2.1 (Poisson-Boltzmann equation). *Suppose that the domain $U \subset \mathbb{R}^d$ is open and bounded, that A is uniformly elliptic, that $\kappa \in L^\infty(U, \mathbb{R}_0^+)$, that $\beta \in \mathbb{R}$ and $\phi_F \in \mathbb{R}$, and that $f \in L^\infty(U)$. Then the boundary-value problem*

$$\begin{aligned} -\nabla \cdot (A\nabla u) + \kappa \sinh(\beta(u-\phi_F)) &= f && \text{in } U, \\ u &= u_D && \text{on } \partial U_D, \\ \nu \cdot \nabla u &= 0 && \text{on } \partial U_N \end{aligned}$$

has a unique solution $u \in H^1(U) \cap L^\infty(U)$. Furthermore, if $f = 0$ almost everywhere, the estimate

$$\min(\inf_{\partial U_D} u_D, \phi_F) \le u(x) \le \max(\sup_{\partial U_D} u_D, \phi_F)$$

holds for all $x \in U$.

The Poisson-Boltzmann equation for arbitrary Fermi levels can be linearized as follows. Taylor expansion of (2.3) in u around a general potential ϕ_0 so that $u - \phi_0 \ll 1$ yields

$$\rho_f(x) = \alpha(x) - \gamma(x)u(x) + O\big((u-\phi_0)^2\big)$$

with

$$\alpha(x) := 2c(x)q \sinh \frac{q(\phi_F - \phi_0)}{k_B T} + \frac{2c(x)q^2\phi_0}{k_B T} \cosh \frac{q(\phi_F - \phi_0)}{k_B T}, \tag{2.4a}$$

$$\gamma(x) := \frac{2c(x)q^2}{k_B T} \cosh \frac{q(\phi_F - \phi_0)}{k_B T}. \tag{2.4b}$$

The advantage of this general form is that the expansion point ϕ_0 is not necessarily equal to the Fermi level ϕ_F [18]. Now the choice

$$Lu(x,\omega) := -\nabla \cdot \big(A(x)\nabla u(x,\omega)\big) + \gamma(x)u(x,\omega), \tag{2.5a}$$

$$\rho(x,\omega) := \rho_i(x,\omega) + \alpha(x) \tag{2.5b}$$

corresponds to the stochastic linearized Poisson-Boltzmann equation

$$-\nabla \cdot \big(A(x)\nabla u(x,\omega)\big) + \gamma(x)u(x,\omega) = \rho(x,\omega) \qquad \text{in } U \times \Omega, \tag{2.6a}$$

$$u(x,\omega) = u_D \qquad \text{on } \partial U \times \Omega \tag{2.6b}$$

for arbitrary Fermi levels. Much of the following pertains to general linear stochastic PDEs of the form (2.1), while the leading application is equation (2.6). Whenever further assumptions on the operator L are necessary, they include the physical situation of (2.4) and (2.6).

Regarding the existence and uniqueness of solutions of (2.6), we mention the following result. A weak formulation of (2.6) is to find $u \in H := H_0^1(U \times \Omega)$, H being a Hilbert space, so that $a(u,v) = \langle \rho, v \rangle$ for all $v \in H$, where a is the bilinear form

$$a(u,v) := \int_\Omega \int_U A(x)\nabla u(x,\omega) \cdot \nabla v(x,\omega) + \gamma(x)u(x,\omega)v(x,\omega) \mathrm{d}x \mathrm{d}P(\omega)$$

and $\rho \in H^{-1}$. Using this weak formulation, it is straightforward to obtain the following proposition using the Lax-Milgram theorem.

PROPOSITION 2.2. *Suppose U is an open and bounded subset of $\mathbb{R}^d$ and (Ω,Σ,P) is a probability space with a bounded domain Ω. Suppose further that $A\in L^\infty(U,\mathbb{R}^{d\times d})$ is uniformly elliptic and that $\gamma\in L^\infty(U)$ is nonnegative. Then the boundary-value problem (2.6) has a unique weak solution $u\in H$ and it depends continuously on $\rho\in H^{-1}$.*

This weak formulation is an extension of the theory of deterministic elliptic equations to random fields with finite variance [1–4,17,23]. Different choices for the Hilbert space H are possible and other theories for stochastic elliptic equations have been developed [15,16,21,24,26,35].

In the following, we consider only operators L that do not depend on the random variable ω, i.e., A depends only on position. Regarding the physical aspects of the problem, this means for Poisson-type equations that random fluctuations in the permittivity A are negligible compared to the random fluctuations in the charge distribution ρ. This is the case in the field-effect sensors considered here, as they rely on changes in the electrostatic potential (cf. Fig. 1.1).

3. The multiscale problem and homogenization

In this section, the multiscale problem and the boundary layer are defined first. Then the main result is stated and proved by a homogenization procedure. Finally, important properties of the resulting limiting equation are shown.

3.1. The boundary layer and its fine structure

We choose a Cartesian coordinate system with coordinates $x=(x_1,x_2,x_3)$ and the domain U is the bounded and open subset $U:=(-L_1,L_1)\times(0,L_2)\times(0,L_3)\subset\mathbb{R}^3$ (cf. Fig. 1.1). The boundary layer is located on the positive side of the plane $x_1=0$ so that x_1 is the direction normal to the surface and x_2 and x_3 are parallel to the surface. The boundary layer at $x_1\geq 0$ is characterized by the charge concentration $\rho(x,\omega)$ which exhibits a random and fast varying spatial structure. Since the fine spatial structure cannot be resolved due to computational constraints—especially in view of the stochastic nature of the problem—, the goal is to replace the original problem (2.6) by a homogenized problem.

We proceed by dividing the two-dimensional interface at $x_1=0$ into periodically repeated two-dimensional cells $\mathcal{C}_k$ by defining

$$\mathcal{C}_k:=\mathcal{C}_{(k_2,k_3)}:=[\epsilon k_2,\epsilon(k_2+1))\times[\epsilon k_3,\epsilon(k_3+1))$$

for $k=(k_2,k_3)\in\mathbb{Z}\times\mathbb{Z}$. The cells $\mathcal{C}_k$ are of size ϵ^2 so that they cover the whole interface, i.e.,

$$[0,L_2)\times[0,L_3)\subset\bigcup_{\substack{1\leq k_2\leq K_2\\ 1\leq k_3\leq K_3}}\mathcal{C}_k$$

holds with $K_2:=\lceil L_2/\epsilon\rceil$ and $K_3:=\lceil L_3/\epsilon\rceil$. We use multi-indices $k=(k_2,k_3)$ with $k_2\in\{0,\ldots,K_2-1\}$ and $k_3\in\{0,\ldots,K_3-1\}$ for the cells $\mathcal{C}_k$, and we denote the total number of cells in the boundary layer by $K:=K_2K_3$ and the index set of the cell indices by $\mathcal{K}:=\{(0,0),\ldots,(K_2-1,K_3-1)\}$ so that $|\mathcal{K}|=K$.

Three-dimensional cells are denoted by $[0,L_1]\times\mathcal{C}_k$. The positive real number $\epsilon\ll 1$ denotes the ratio of the cell size to the whole simulation domain U. We use a homogenization ansatz where we scale the boundary layer by introducing fast variables. We stretch the x_1-, x_2-, and x_3-coordinates at the interface $x_1=0$ by a factor of $1/\epsilon$ and hence obtain the fast variables $\eta_1:=x_1/\epsilon$, $\eta_2:=x_2/\epsilon$, and $\eta_3:=x_3/\epsilon$ in

contrast to the slow variables x_1, x_2, and x_3. The idea of the multiscale ansatz is to write the charge concentration ρ^ϵ as a function

$$\rho^\epsilon = \frac{1}{\epsilon^2}\rho\Big(\frac{x_1}{\epsilon},\frac{x_2}{\epsilon},\frac{x_3}{\epsilon},x_2,x_3,\omega\Big) = \frac{1}{\epsilon^2}\rho(\eta_1,\eta_2,\eta_3,x_2,x_3,\omega) \tag{3.1}$$

of both the fast and the slow variables. The dependence of ρ on the slow variables x_2 and x_3 includes slow variations in the boundary layer. Furthermore, the function ρ is quasi-periodic: it is 1-periodic in its second argument η_2 and in its third argument η_3, i.e., the equation

$$\rho(\eta_1,\eta_2,\eta_3,x_2,x_3,\omega) = \rho(\eta_1,\eta_2+k_2,\eta_3+k_3,x_2,x_3,\omega) \qquad \forall (k_2,k_3)\in\mathbb{Z}\times\mathbb{Z} \tag{3.2}$$

holds. This is consistent with the definition of the cells $\mathcal{C}_k$. Additionally, the charges in the boundary layer are concentrated close to the interface at $x_1 = 0$, i.e.,

$$\lim_{\eta_1\to\infty}\rho(\eta_1,\eta_2,\eta_3,x_2,x_3) = 0 \tag{3.3}$$

holds.

The significance of the factor $1/\epsilon^2$ in the multiscale ansatz (3.1) is explained after Corollary 3.4 at the end of this section, where an alternative scaling is discussed as well.

We now describe the dependence of the charge concentration ρ on the random variable ω. For each cell $\mathcal{C}_k$, there is a random variable ω_k so that the charge concentration ρ_k of the cell $\mathcal{C}_k$ depends on ω_k. In reality, the different states of the random variable ω_k correspond to the presence of different molecules and to different orientations thereof the boundary layer. We define the random variable

$$\omega := (\omega_1,\dots,\omega_K)$$

that includes the states of all cells in the boundary layer. It is assumed that the molecules in each cell do not affect the molecules in the other cells. This assumption is satisfied in realistic structures, since their distance is large enough to ensure full electrostatic screening, and it is well supported by Monte-Carlo simulations [14] and Poisson-Boltzmann simulations [32] of screening. Thus we assume that ρ_k and ρ_ℓ are independent for $k\neq\ell$ and hence uncorrelated, i.e.,

$$k\neq\ell \Longrightarrow \operatorname{cov}\big(\rho_k(y,.),\rho_\ell(z,.)\big) = 0 \qquad \forall y,z\in U, \quad \forall k,\ell\in\mathcal{K}.$$

In other words, $(\rho_1,\dots,\rho_K)$ is a K-dimensional random vector with mutually independent components.

In the following, we will need the definition of a joint moment.

DEFINITION 3.1 (joint moment). *Suppose α is a multi-index of dimension $J := \dim\alpha$. The joint moment M_α of the J random variables X_j is defined as*

$$M_\alpha(X_1,\dots,X_J) := E\Big(\prod_{j=1}^{J}(X_j - EX_j)^{\alpha_j}\Big).$$

The covariance of two random variables X_1 and X_2 is defined as $\operatorname{cov}(X_1,X_2) := M_{(1,1)}(X_1,X_2)$. To simplify notation, we write

$$(\operatorname{cov} u)(x,y) := \operatorname{cov}\big(u(x,.),u(y,.)\big)$$

for the covariance of u evaluated at x and $y\in U$. In the following, we denote centered random variables by $\tilde{X}$, i.e., $\tilde{X} := X - EX$.

3.2. The main result and the limiting equations

In order to state the main result, the following assumptions are needed.

ASSUMPTIONS 3.2.

(i) *The domain $U \subset \mathbb{R}^3$ is open and bounded.*
(ii) *The function $\rho \in L^\infty(U)$ satisfies (3.2) and (3.3).*
(iii) *The functions ρ_k and ρ_ℓ are uncorrelated for $k \neq \ell$.*
(iv) *The linear differential operator L is independent of ϵ and has a sufficiently smooth Green's function G.*

The assumption on the linear operator L includes the important case of elliptic operators. The following result will be shown formally.

THEOREM 3.3 (limiting problem for the covariance). *Suppose that Assumptions 3.2 hold. Then the limiting problem as $\epsilon \to 0+$ for the covariance of the solutions u_ϵ of the boundary-value problem*

$$Lu_\epsilon(x,\omega) = \rho^\epsilon(x,\omega) \quad \text{in } U, \tag{3.4a}$$
$$u = u_D \quad \text{on } \partial U \tag{3.4b}$$

is the boundary-value problem

$$L_z L_y(\operatorname{cov} u)(y,z) = \delta(y_1,z_1,y_2-z_2,y_3-z_3)\bar{R}(y_2,y_3)^2 \quad \text{in } U \times U, \tag{3.5a}$$
$$\operatorname{cov} u = 0 \quad \text{on } \partial U \times U, \tag{3.5b}$$
$$\operatorname{cov} u = 0 \quad \text{on } U \times \partial U \tag{3.5c}$$

for $\operatorname{cov} u$, where $\bar{R}$ is defined by

$$R(k,\omega_k) := \int_0^\infty \int_0^1 \int_0^1 \tilde{\rho}_k(\eta_1,\eta_2,\eta_3,\omega_k)\mathrm{d}\eta_3\eta_2\eta_1, \tag{3.6a}$$
$$\bar{R}(\epsilon k_2, \epsilon k_3) := \left(\int_\Omega R(k,\omega_k)^2 \mathrm{d}P(\omega_k) \right)^{1/2}. \tag{3.6b}$$

Note that due to the delta distributions on the right-hand side of (3.5a), the equation is symmetric in y and z.

Proof. To simplify the calculations, we will use the centered solution $\tilde{u}$ and the centered right-hand sides $\tilde{\rho}_k$ and $\tilde{\rho}$. For the centered quantities, the identities $E\tilde{u} = 0$, $E\tilde{\rho} = 0$, $E\tilde{\rho}_k = 0$, and

$$\tilde{\rho}(x,\omega) = \sum_{k \in \mathcal{K}} \chi_k(x)\tilde{\rho}_k(x,\omega_k) \tag{3.7}$$

hold, where $\chi_k(x)$ is the characteristic function of the cell $\mathcal{C}_k$. We immediately find

$$L\tilde{u}_\epsilon = \tilde{\rho}^\epsilon. \tag{3.8}$$

It is straightforward to show that the equations $\operatorname{cov} u_\epsilon = \operatorname{cov} \tilde{u}_\epsilon$ and $\operatorname{var} u_\epsilon = \operatorname{var} \tilde{u}_\epsilon$ hold for the centered covariance and variance.

G is a Green's function of L on U, i.e.,

$$LG(x,y) = \delta(x-y) \quad \forall x,y \in U$$

holds. Note that L and therefore G is independent of ϵ. Using the Green's function G, the solution $\tilde{u}$ of (3.8) is given by

$$\tilde{u}_\epsilon(x,\omega) = \int_U G(x,y)\tilde{\rho}^\epsilon(y,\omega)\mathrm{d}y.$$

To calculate the joint moments of $X_j := \tilde{u}(x_j,\omega)$, we first write the integrand as

$$\prod_{j=1}^{J} \tilde{u}_\epsilon(x_j,\omega)^{\alpha_j} = \int_{U^{|\alpha|}} \prod_{j=1}^{J} \prod_{\nu=1}^{\alpha_j} \big(G(x_j,\xi_{j\nu})\tilde{\rho}^\epsilon(\xi_{j\nu},\omega)\big) \mathrm{d}\xi_{11}\ldots\xi_{1\alpha_1}\ldots\xi_{J1}\ldots\xi_{J\alpha_J},$$

where $|\alpha| = \sum_{j=1}^{J} \alpha_j$, and use (3.7) to find

$$\begin{aligned} M_\alpha\big(\tilde{u}_\epsilon(x_j,\omega)\big) &= \int_\Omega \prod_{j=1}^{J} \tilde{u}_\epsilon(x_j,\omega)^{\alpha_j} \mathrm{d}P(\omega) \\ &= \int_\Omega \int_{U^{|\alpha|}} \prod_{j=1}^{J} \prod_{\nu=1}^{\alpha_j} \big(G(x_j,\xi_{j\nu}) \sum_{k_{j\nu}\in\mathcal{K}} \chi_{k_{j\nu}}(\xi_{j\nu})\tilde{\rho}^\epsilon_{k_{j\nu}}(\xi_{j\nu},\omega_{k_{j\nu}})\big) \mathrm{d}\xi_{11}\ldots\xi_{J\alpha_J}\mathrm{d}P(\omega). \end{aligned}$$

We denote the characteristic function of the interval $[0,1)$ by χ and hence we have

$$\chi_k(x) = \chi_{(k_2,k_3)}(x_2,x_3) = \chi\Big(\frac{x_2}{\epsilon} - k_2\Big)\chi\Big(\frac{x_3}{\epsilon} - k_3\Big)$$

for the characteristic function χ_k of cell $\mathcal{C}_k$. Now the moment M_α is given by

$$\begin{aligned} M_\alpha\big(\tilde{u}_\epsilon(x_j,\omega)\big) &= \int_\Omega \int_{U^{|\alpha|}} \Big(\prod_{j=1}^{J} \prod_{\nu=1}^{\alpha_j} G(x_j,\xi_{j\nu})\Big) \cdot \\ &\cdot \sum_{k_{11}\in\mathcal{K}} \cdots \sum_{k_{J\alpha_J}\in\mathcal{K}} \chi_{k_{11}}(\xi_{11})\cdots\chi_{k_{J\alpha_J}}(\xi_{J\alpha_J})\tilde{\rho}^\epsilon_{k_{11}}(\xi_{11},\omega_{k_{11}})\cdots\tilde{\rho}^\epsilon_{k_{J\alpha_J}}(\xi_{J\alpha_J},\omega_{k_{J\alpha_J}}) \\ &\qquad \mathrm{d}\xi_{11}\ldots\xi_{J\alpha_J}\mathrm{d}P(\omega) \\ &= \sum_{k_{11}\in\mathcal{K}} \cdots \sum_{k_{J\alpha_J}\in\mathcal{K}} \int_\Omega \int_0^\infty \int_{\epsilon k_{11,2}}^{\epsilon(k_{11,2}+1)} \int_{\epsilon k_{11,3}}^{\epsilon(k_{11,3}+1)} \cdots \\ &\qquad \cdots \int_0^\infty \int_{\epsilon k_{J\alpha_J,2}}^{\epsilon(k_{J\alpha_J,2}+1)} \int_{\epsilon k_{J\alpha_J,3}}^{\epsilon(k_{J\alpha_J,3}+1)} \\ &\Big(\prod_{j=1}^{J} \prod_{\nu=1}^{\alpha_j} G(x_j,\xi_{j\nu})\Big)\tilde{\rho}^\epsilon_{k_{11}}(\xi_{11},\omega_{k_{11}})\cdots\tilde{\rho}^\epsilon_{k_{J\alpha_J}}(\xi_{J\alpha_J},\omega_{k_{J\alpha_J}}) \\ &\qquad \mathrm{d}\xi_{J\alpha_J,3}\xi_{J\alpha_J,2}\xi_{J\alpha_J,1}\ldots\xi_{11,3}\xi_{11,2}\xi_{11,1}\mathrm{d}P(\omega). \end{aligned}$$

We use the multiscale ansatz from §3.1 for $\tilde{\rho}^\epsilon_k$ so that

$$\begin{aligned} \tilde{\rho}^\epsilon_k(x,\omega_k) &= \frac{1}{\epsilon^2}\tilde{\rho}_k\Big(\frac{x_1}{\epsilon}, \frac{x_2}{\epsilon} - k_2, \frac{x_3}{\epsilon} - k_3, \omega_k\Big) \\ &= \frac{1}{\epsilon^2}\tilde{\rho}\Big(\frac{x_1}{\epsilon}, \frac{x_2}{\epsilon} - k_2, \frac{x_3}{\epsilon} - k_3, \epsilon k_2, \epsilon k_3, \omega_k\Big). \end{aligned}$$

The function $\tilde{\rho}_k$ depends on the cell index k, whereas $\tilde{\rho}$ depends on the slow variables $x_2 = \epsilon k_2$ and $x_3 = \epsilon k_3$ instead of the cell index k.

For the moment M_α, this yields

$$M_\alpha\big(\tilde u_\epsilon(x_j,\omega)\big)=\epsilon^{-2|\alpha|}\sum_{k_{11}\in\mathcal{K}}\dots\sum_{k_{J\alpha_J}\in\mathcal{K}}\int_\Omega\int_0^\infty\int_{\epsilon k_{11,2}}^{\epsilon(k_{11,2}+1)}\int_{\epsilon k_{11,3}}^{\epsilon(k_{11,3}+1)}\dots$$
$$\dots\int_0^\infty\int_{\epsilon k_{J\alpha_J,2}}^{\epsilon(k_{J\alpha_J,2}+1)}\int_{\epsilon k_{J\alpha_J,3}}^{\epsilon(k_{J\alpha_J,3}+1)}\Bigg(\prod_{j=1}^{J}\prod_{\nu=1}^{\alpha_j}G(x_j,\xi_{j\nu})\Bigg)\cdot$$
$$\cdot\tilde\rho_{k_{11}}\Big(\tfrac{\xi_{11,1}}{\epsilon},\tfrac{\xi_{11,2}}{\epsilon}-k_2,\tfrac{\xi_{11,3}}{\epsilon}-k_3,\omega_{k_{11}}\Big)\cdots\tilde\rho_{k_{J\alpha_J}}\Big(\tfrac{\xi_{J\alpha_J,1}}{\epsilon},\tfrac{\xi_{J\alpha_J,2}}{\epsilon}-k_2,\tfrac{\xi_{J\alpha_J,3}}{\epsilon}-k_3,\omega_{k_{J\alpha_J}}\Big)$$
$$\mathrm{d}\xi_{J\alpha_J,3}\xi_{J\alpha_J,2}\xi_{J\alpha_J,1}\dots\xi_{11,3}\xi_{11,2}\xi_{11,1}\mathrm{d}P(\omega).\quad(3.9)$$

After substituting

$$\bar\xi_{j\nu,1}:=\frac{1}{\epsilon}\xi_{j\nu,1},$$
$$\bar\xi_{j\nu,2}:=\frac{1}{\epsilon}\xi_{j\nu,2}-k_{j\nu,2},$$
$$\bar\xi_{j\nu,3}:=\frac{1}{\epsilon}\xi_{j\nu,3}-k_{j\nu,3}$$

and renaming, we find

$$M_\alpha\big(\tilde u_\epsilon(x_j,\omega)\big)=\epsilon^{|\alpha|}\sum_{k_{11}\in\mathcal{K}}\dots\sum_{k_{J\alpha_J}\in\mathcal{K}}\int_\Omega\int_0^\infty\int_0^1\int_0^1\dots\int_0^\infty\int_0^1\int_0^1$$
$$\Bigg(\prod_{j=1}^{J}\prod_{\nu=1}^{\alpha_j}G\big(x_j,(\epsilon\xi_{j\nu,1},\epsilon(\xi_{j\nu,2}+k_{j\nu,2}),\epsilon(\xi_{j\nu,3}+k_{j\nu,3}))\big)\Bigg)\cdot$$
$$\cdot\tilde\rho_{k_{11}}(\xi_{11},\omega_{k_{11}})\cdots\tilde\rho_{k_{J\alpha_J}}(\xi_{J\alpha_J},\omega_{k_{J\alpha_J}})$$
$$\mathrm{d}\xi_{J\alpha_J,3}\xi_{J\alpha_J,2}\xi_{J\alpha_J,1}\dots\xi_{11,3}\xi_{11,2}\xi_{11,1}\mathrm{d}P(\omega).\quad(3.10)$$

The product involving the Green's function G on the right-hand side can be simplified by noting that L and hence G do not depend on ϵ (apart from the arguments above) and that G is smooth enough by assumption. Since $\xi_{j\nu,i}\in[0,1]$, $\epsilon\xi_{j\nu,i}=O(\epsilon)$ holds for all $i\in\{1,\dots,d\}$. Furthermore, $k_{j\nu,i}=O(1/\epsilon)$ holds for $i\in\{2,3\}$ by the definition of K_i and therefore $\epsilon k_{j\nu,i}=O(1)$. Hence Taylor expansion of the Green's function G yields

$$G\big(x_j,(\epsilon\xi_{j\nu,1},\epsilon(\xi_{j\nu,2}+k_{j\nu,2}),\epsilon(\xi_{j\nu,3}+k_{j\nu,3}))\big)$$
$$=G\big(x_j,(0,\epsilon k_{j\nu,2},\epsilon k_{j\nu,3})\big)+\epsilon\xi_{j\nu}\cdot\nabla_2G\big(x_j,(0,\epsilon k_{j\nu,2},\epsilon k_{j\nu,3})\big)+O(\epsilon^2),$$

where ∇_2 denotes the gradient with respect to the second variable.

We therefore obtain

$$M_\alpha\big(\tilde u_\epsilon(x_j,\omega)\big)=\epsilon^{|\alpha|}\sum_{k_{11}\in\mathcal{K}}\dots\sum_{k_{J\alpha_J}\in\mathcal{K}}\int_\Omega\int_0^\infty\int_0^1\int_0^1\dots\int_0^\infty\int_0^1\int_0^1$$
$$\Bigg(\prod_{j=1}^{J}\prod_{\nu=1}^{\alpha_j}G\big(x_j,(0,\epsilon k_{j\nu,2},\epsilon k_{j\nu,3})\big)\Bigg)\tilde\rho_{k_{11}}(\xi_{11},\omega_{k_{11}})\cdots\tilde\rho_{k_{J\alpha_J}}(\xi_{J\alpha_J},\omega_{k_{J\alpha_J}})$$
$$\mathrm{d}\xi_{J\alpha_J,3}\xi_{J\alpha_J,2}\xi_{J\alpha_J,1}\dots\xi_{11,3}\xi_{11,2}\xi_{11,1}\mathrm{d}P(\omega)+O(\epsilon^{|\alpha|+1})\quad(3.11)$$

and further

$$M_\alpha\big(\tilde u_\epsilon(x_j,\omega)\big)=\epsilon^{|\alpha|}\sum_{k_{11}\in\mathcal{K}}\dots\sum_{k_{J\alpha_J}\in\mathcal{K}}\prod_{j=1}^{J}\prod_{\nu=1}^{\alpha_j}G\big(x_j,(0,\epsilon k_{j\nu,2},\epsilon k_{j\nu,3})\big)\cdot$$
$$\cdot\int_0^\infty\int_0^1\int_0^1\dots\int_0^\infty\int_0^1\int_0^1 M_\alpha(\tilde\rho_{k_{11}},\dots,\tilde\rho_{k_{J\alpha_J}})\mathrm{d}\xi_{J\alpha_J}\dots\xi_{11}+O(\epsilon^{|\alpha|+1})\quad(3.12)$$

for $|\alpha_j|\le 1$ for all $j\in\{1,\dots,J\}$. This is a general representation of the joint moment $M_\alpha(\tilde u(x_j,\omega))$ of $\tilde u(x_j,\omega)$ in terms of the joint moment $M_\alpha(\tilde\rho_{k_{j\nu}})$ of the data ρ.

To obtain specific results for the covariance $M_{(1,1)}$, we use that $\tilde\rho_k$ and $\tilde\rho_\ell$ are uncorrelated for $k\neq\ell$. This implies

$$\int_\Omega\tilde\rho_k(y,\omega_k)\tilde\rho_\ell(z,\omega_\ell)\mathrm{d}P(\omega)=\delta_{k\ell}\int_\Omega\tilde\rho_k(y,\omega_k)\tilde\rho_k(z,\omega_k)\mathrm{d}P(\omega)\quad\forall y,z\in U,$$

where $\delta_{k\ell}$ is the Kronecker delta. Using this last equation and definition (3.6a) of R, the covariance simplifies to

$$\begin{aligned}(\mathrm{cov}\,u_\epsilon)(y,z)&=M_{(1,1)}\big(\tilde u_\epsilon(y,\omega),\tilde u_\epsilon(z,\omega)\big)\\&=\epsilon^2\sum_{k\in\mathcal{K}}\sum_{\ell\in\mathcal{K}}G\big(y,(0,\epsilon k_2,\epsilon k_3)\big)G\big(z,(0,\epsilon\ell_2,\epsilon\ell_3)\big)\cdot\\&\cdot\int_0^\infty\int_0^1\int_0^1\int_0^\infty\int_0^1\int_0^1\int_\Omega\tilde\rho_k(y,\omega_k)\tilde\rho_\ell(z,\omega_\ell)\mathrm{d}P(\omega)\mathrm{d}z_3z_2z_1y_3y_2y_1+O(\epsilon^3)\\&=\epsilon^2\sum_{k\in\mathcal{K}}G\big(y,(0,\epsilon k_2,\epsilon k_3)\big)G\big(z,(0,\epsilon k_2,\epsilon k_3)\big)\cdot\\&\cdot\int_0^\infty\int_0^1\int_0^1\int_0^\infty\int_0^1\int_0^1\int_\Omega\tilde\rho_k(y,\omega_k)\tilde\rho_k(z,\omega_k)\mathrm{d}P(\omega)\mathrm{d}z_3z_2z_1y_3y_2y_1+O(\epsilon^3)\\&=\epsilon^2\sum_{k\in\mathcal{K}}G\big(y,(0,\epsilon k_2,\epsilon k_3)\big)G\big(z,(0,\epsilon k_2,\epsilon k_3)\big)\int_\Omega R(k,\omega_k)^2\mathrm{d}P(\omega_k)+O(\epsilon^3).\quad(3.13)\end{aligned}$$

We convert the Riemann sum over k_2 and k_3 into a two-dimensional integral over y_2 and y_3 to find

$$(\mathrm{cov}\,u_\epsilon)(y,z)=\int_0^{L_3}\int_0^{L_2}G\big(y,(0,x_2,x_3)\big)G\big(z,(0,x_2,x_3)\big)\bar R(x_2,x_3)^2\mathrm{d}x_2x_3+O(\epsilon).\quad(3.14)$$

Here $\bar R$ is defined by (3.6b) and it is evaluated at the point (x_2,x_3) that lies in cell $k=(k_2,k_3)$ determined by the equations $x_2=\epsilon k_2$ and $x_3=\epsilon k_3$.

Finally, we apply L_y, i.e., the operator L with derivatives with respect to y, to find

$$\begin{aligned}&L_y(\mathrm{cov}\,u_\epsilon)(y,z)\\&\quad=\int_0^{L_3}\int_0^{L_2}\delta(y_1,y_2-x_2,y_3-x_3)G\big(z,(0,x_2,x_3)\big)\bar R(x_2,x_3)^2\mathrm{d}x_2x_3+O(\epsilon),\end{aligned}$$

and we apply L_z, the operator with respect to z, to find

$$\begin{aligned}
&L_z L_y(\operatorname{cov} u)(y,z)\\
&=\int_0^{L_3}\int_0^{L_2}\delta(y_1,y_2-x_2,y_3-x_3)\delta(z_1,z_2-x_2,z_3-x_3)\bar{R}(x_2,x_3)^2\mathrm{d}x_2x_3\\
&=\delta(y_1,z_1,y_2-z_2,y_3-z_3)\bar{R}(y_2,y_3)^2.
\end{aligned}$$

This concludes the proof. □

Note that due to the factor $\delta(y_1,z_1)$ on the right-hand side, the covariance is concentrated at the interface $x_1=0$. Regarding the physics of the problem, R can be interpreted as the surface-charge density of the boundary layer as a function of the slow variables for a given ω_k. Then $\bar{R}^2$ is the variance of the surface-charge density R.

The proof also yields the following rate when the scaling (3.1) is replaced by the alternative scaling (3.15).

Corollary 3.4 (rate for the covariance). *Under Assumptions 3.2, but with the scaling*

$$\rho^\epsilon=\rho\Big(\frac{x_1}{\epsilon},\frac{x_2}{\epsilon},\frac{x_3}{\epsilon},x_2,x_3,\omega\Big)=\rho(y_1,y_2,y_3,x_2,x_3,\omega) \tag{3.15}$$

instead of the previous scaling (3.1), the covariance $\operatorname{cov}\tilde{u}=\operatorname{cov}u$ *scales like* ϵ^4 *as* $\epsilon\to 0$.

Proof. The corollary follows by inspecting the proof of Theorem 3.3 and making the changes due to the new scaling (3.15). In equation (3.9), the factor $\epsilon^{-2|\alpha|}$ becomes 1 now. In equation (3.10), the factor $\epsilon^{|\alpha|}$ becomes $\epsilon^{3|\alpha|}$. In equations (3.11) and (3.12), the factor $\epsilon^{|\alpha|}$ becomes $\epsilon^{3|\alpha|}$ and the order becomes $O(\epsilon^{3|\alpha|+1})$. In equation (3.13), the factor ϵ^6 becomes ϵ^2 and the order becomes $O(\epsilon^7)$. In equation (3.14) and in the remaining equations, there is an additional factor ϵ^4 now and the order is $O(\epsilon^5)$. □

The difference compared to the previous scaling in (3.1) is the omission of the factor $1/\epsilon^2$. The interpretation of the two cases is that in the scaling in (3.1) the charge concentration is increased by the factor $1/\epsilon^2$ as $\epsilon\to 0+$ so that the right-hand side in equation (3.5a) is precisely of order $O(1)$. In the alternative scaling in (3.15), the cells just become smaller, but the charge concentration is not increased. Since there is no additional factor, the right-hand side in equation (3.5a) converges to zero as $\epsilon\to 0+$. Hence the covariance and variance vanish as well and the present corollary gives the rate as ϵ^4.

3.3. Existence, uniqueness, and further properties

Having found the limiting problem, the properties of its solution are investigated here. It is expected that its solution, being interpreted as a covariance, is unique. A priori bounds are also given. Furthermore, it will be shown that the covariance is symmetric as expected.

Since the covariance is symmetric in its two arguments by definition, it is expected that symmetry is preserved by homogenization, i.e., that the solution $\operatorname{cov}u$ of the homogenized equation (3.5a) in Theorem 3.3 is symmetric in y and z. This is indeed the case as shown in the following proposition. For notational simplicity we write u for $\operatorname{cov}u$.

Proposition 3.5. *Suppose that the boundary conditions of the boundary-value problem*

$$L_zL_yu(y,z)=f(y,z)$$

and the right-hand side f are symmetric in y and z and that u is a weak solution of this problem. Then u is symmetric a.e.

Proof. We denote the symmetric part of $u(y,z)$ by $v(y,z) := \big(u(y,z)+u(z,y)\big)/2$ and its antisymmetric part by $w(y,z) := \big(u(y,z)-u(z,y)\big)/2$. The weak formulation of the problem is

$$\iint L_y u(y,z) L_z^* \phi(y,z) - f(y,z)\phi(y,z)\mathrm{d}yz = 0 \tag{3.16}$$

for all test functions ϕ. Interchanging y and z yields

$$\iint L_z u(z,y) L_y^* \phi(z,y) - f(z,y)\phi(z,y)\mathrm{d}yz = 0$$

and swapping L_y and L_z using their adjoints, using the symmetry of f, and replacing $\phi(z,y)$ by $\phi(y,z)$ (since the equation holds for all test functions) yields

$$\iint L_y u(z,y) L_z^* \phi(y,z) - f(y,z)\phi(y,z)\mathrm{d}yz = 0. \tag{3.17}$$

Finally subtracting (3.17) from (3.16) yields $\iint L_y w(y,z) L_z^* \phi(y,z)\mathrm{d}yz = 0$ and hence

$$\iint w(y,z) L_y^* L_z^* \phi(y,z)\mathrm{d}yz = 0$$

holds for all test functions ϕ. Therefore the antisymmetric part w vanishes a.e. □

PROPOSITION 3.6. *Suppose that $U \subset \mathbb{R}^d$ is an open and bounded domain and that ∂U is C^2, suppose that $f \in H^{-1}(U\times U)$, and suppose that $L_x = -\nabla_x \cdot (A(x)\nabla_x)$ is an elliptic operator with $a_{ij} \in C^1(\bar{U})$ and that A is uniformly elliptic with constant α. Then the boundary-value problem*

$$\begin{aligned} L_z L_y u(y,z) &= f(y,z) && \text{in } U\times U,\\ u(y,z) &= 0 && \text{on } \partial U \times U,\\ u(y,z) &= 0 && \text{on } U \times \partial U \end{aligned}$$

has a unique solution $u \in H^1(U\times U)$ and the estimate

$$\|u\|_{H^1(U\times U)} \le \frac{\sqrt{2}}{\alpha^2}\|f\|_{H^{-1}(U\times U)}$$

holds.

Proof. We use the Lax-Milgram theorem twice. First, we consider the boundary-value problem $L_z w(y,z) = f(y,z)$ for all $y \in U$. It has a unique solution $w(y,.) \in H^2(U)$ for all $y \in U$, since $f \in H^{-1}(U\times U)$ and the data are smooth, and the inequality

$$\|w\|_{L^2(U\times U)} \le \frac{1}{\alpha}\|f\|_{H^{-1}(U\times U)} \tag{3.18}$$

follows immediately.

Second, we consider the boundary-value problem $L_y u(y,z) = w(y,z)$ for all $z \in U$. Similarly, it has a unique solution $u(.,z) \in H^2(U)$ for all $z \in U$ and the estimate

$$\|u(.,z)\|_{H^2(U)} \le \frac{1}{\alpha}\|w(.,z)\|_{L^2(U)} \tag{3.19}$$

holds for all $z \in U$.

Third, the problem $L_y L_z u(y,z) = f(y,z)$ is equivalent to the original problem (note that L_y and L_z are interchanged). To show this claim, we calculate using the definition of the weak derivative that

$$\int_U (L_z L_y u)\phi \mathrm{d}y\mathrm{d}z = \int_U u L_y^* L_z^* \phi \mathrm{d}y\mathrm{d}z = \int_U u L_z^* L_y^* \phi \mathrm{d}y\mathrm{d}z = \int_U (L_y L_z u)\phi \mathrm{d}y\mathrm{d}z$$

for all $\phi \in C_c^\infty(U)$. Therefore the equation $L_z L_y u = L_y L_z u$ holds a.e. This yields the symmetric estimate

$$\|u(y,.)\|_{H^2(U)} \leq \frac{1}{\alpha} \|w(y,.)\|_{L^2(U)} \tag{3.20}$$

for all $y \in U$.

Finally, these three inequalities yield the asserted estimate: Integrating estimate (3.19) with respect to z and (3.20) with respect to y gives

$$\|u\|_{H^1(U\times U)}^2 \leq \frac{2}{\alpha^2} \|w\|_{L^2(U\times U)}^2,$$

and this inequality with (3.18) concludes the proof. □

To see that Proposition 3.6 applies to the limiting problem in Theorem 3.3, we set

$$f(y,z) := \delta(y_1, z_1, y_2 - z_2, y_3 - z_3) g(y_2, y_3),$$

where $g \in L^2(U \times U)$. We define a functional F and calculate

$$\begin{aligned} F(v) &:= \int_U \int_U f(y,z) v(y,z) \mathrm{d}y\mathrm{d}z \\ &= \int_U \int_U \delta(y_1, z_1, y_2 - z_2, y_3 - z_3) g(y_2, y_3) v(y,z) \mathrm{d}y\mathrm{d}z \\ &= \iint g(y_2, y_3) v(0, y_2, y_3, 0, y_2, y_3) \mathrm{d}y_2 \mathrm{d}y_3. \end{aligned}$$

If $v \in H^1(U \times U)$, then $F(v)$ is bounded by the Cauchy-Schwarz inequality and hence $f \in H^{-1}(U \times U)$.

4. Numerical approximation

In this section, a discretization for the limiting problem for the covariance in Theorem 3.3 is given in the important case where the original equation is the Poisson equation. Furthermore, numerical results as obtained by Monte-Carlo solutions are presented as a verification of the rate in Corollary 3.4.

4.1. A compact fourth-order FD discretization for the covariance equation for the stochastic Poisson equation

In view of the fact that the covariance equation lives on twice the dimensions than the original problem, a discretization of high order is advantageous. In the following, we consider the Laplace operator

$$L := \Delta$$

in two spatial dimensions and use the fourth-order discretization

$$\begin{bmatrix} \frac{1}{6} & \frac{2}{3} & \frac{1}{6} \\ \frac{2}{3} & -\frac{10}{3} & \frac{2}{3} \\ \frac{1}{6} & \frac{2}{3} & \frac{1}{6} \end{bmatrix}_{i,j} u_{i,j} = h^2 \begin{bmatrix} 0 & \frac{1}{12} & 0 \\ \frac{1}{12} & \frac{2}{3} & \frac{1}{12} \\ 0 & \frac{1}{12} & 0 \end{bmatrix}_{i,j} f_{i,j} \tag{4.1}$$

of the equation $\Delta u = f$. The values in the brackets indicate 9-point discretization stars, and the indices (i,j) indicate that the discretization star is applied to these variables. This discretization has a fourth-order truncation error and is often called compact, since it only involves neighboring grid points of (i,j).

PROPOSITION 4.1 (Fourth-order compact FD scheme for the 2d Poisson equation). *The local truncation error of the FD scheme in (4.1) for the 2d Poisson equation $\Delta u = f$ is of fourth order.*

Proof. We denote the (second-order) central-difference operator with respect to x by

$$D_x^2 u_{i,j} := \frac{u_{i+1,j} - 2u_{i,j} + u_{i-1,j}}{h^2}.$$

Taylor expansion around $u_{i,j}$ yields

$$D_x^2 u_{i,j} = u_{xx} + \frac{h^2}{12} u_{xxxx} + O(h^4)$$

and therefore the truncation error $\tau_{i,j}$ in the discretization

$$D_x^2 u_{i,j} + D_y^2 u_{i,j} = f_{i,j} + \tau_{i,j}$$

of the 2d Poisson equation equals

$$\tau_{i,j} = \frac{h^2}{12}(u_{xxxx} + u_{yyyy}) + O(h^4).$$

In order to obtain more information about the second-order term in the last equation, we differentiate the Poisson equation to find

$$\begin{aligned} u_{xxxx} &= f_{xx} - u_{xxyy}, \\ u_{yyyy} &= f_{yy} - u_{xxyy} \end{aligned}$$

and can rewrite the truncation error as

$$\tau_{i,j} = \frac{h^2}{12}(f_{xx} + f_{yy}) - \frac{h^2}{6} u_{xxyy} + O(h^4). \tag{4.2}$$

Approximating its second-order terms by the second-order schemes

$$\begin{aligned} f_{xx} &= D_x^2 f_{i,j} + O(h^2), \\ u_{xxyy} &= D_x^2 D_y^2 u_{i,j} + O(h^2), \end{aligned}$$

the second-order terms in (4.2) are eliminated and the discretization becomes fourth order. In summary, the FD discretization is

$$D_x^2 u_{i,j} + D_y^2 u_{i,j} + \frac{h^2}{6} D_x^2 D_y^2 u_{i,j} = f_{i,j} + \frac{h^2}{12}(D_x^2 + D_y^2) f_{i,j} + O(h^4)$$

and some manipulations yield (4.1). □

Using Proposition 4.1, a discretization of the covariance equation (3.5) for $L=\Delta$ is given by

$$\begin{bmatrix} \frac{1}{6} & \frac{2}{3} & \frac{1}{6} \\ \frac{2}{3} & -\frac{10}{3} & \frac{2}{3} \\ \frac{1}{6} & \frac{2}{3} & \frac{1}{6} \end{bmatrix}_{i,j} \begin{bmatrix} \frac{1}{6} & \frac{2}{3} & \frac{1}{6} \\ \frac{2}{3} & -\frac{10}{3} & \frac{2}{3} \\ \frac{1}{6} & \frac{2}{3} & \frac{1}{6} \end{bmatrix}_{k,l} u_{i,j,k,l} = h^4 \begin{bmatrix} 0 & \frac{1}{12} & 0 \\ \frac{1}{12} & \frac{2}{3} & \frac{1}{12} \\ 0 & \frac{1}{12} & 0 \end{bmatrix}_{i,j} \begin{bmatrix} 0 & \frac{1}{12} & 0 \\ \frac{1}{12} & \frac{2}{3} & \frac{1}{12} \\ 0 & \frac{1}{12} & 0 \end{bmatrix}_{k,l} f_{i,j,k,l}.$$

This discretization is a fourth-order scheme and only neighboring grid points are used, which simplifies the implementation of boundary conditions. It has 81 terms for u on the left-hand side and 25 terms for f on the right-hand side.[1]

In Figures 4.1 and 4.2, variances are calculated for two different right-hand sides. The 2d variances are calculated as the diagonals of the 2×2-dimensional covariance problem. As expected, the variances are nonnegative and have their global maximum where the covariance of the data is concentrated.

In three spatial dimensions, the following proposition is useful.

PROPOSITION 4.2 (Fourth-order compact FD scheme for the 3d Poisson equation). *The local truncation error of the FD scheme*

$$\begin{aligned} &-4u_{i,j,k}+\tfrac{1}{3}(u_{i+1,j,k}+u_{i-1,j,k}+u_{i,j+1,k}+u_{i,j-1,k}+u_{i,j,k+1}+u_{i,j,k-1}) \\ &\quad+\tfrac{1}{6}(+u_{i,j+1,k+1}+u_{i,j+1,k-1}+u_{i,j-1,k+1}+u_{i,j-1,k-1} \\ &\qquad+u_{i+1,j,k+1}+u_{i+1,j,k-1}+u_{i-1,j,k+1}+u_{i-1,j,k-1} \\ &\qquad+u_{i+1,j+1,k}+u_{i+1,j-1,k}+u_{i-1,j+1,k}+u_{i-1,j-1,k}) \\ &=h^2\big(\tfrac{1}{2}f_{i,j,k}+\tfrac{1}{12}(f_{i+1,j,k}+f_{i-1,j,k}+f_{i,j+1,k}+f_{i,j-1,k}+f_{i,j,k+1}+f_{i,j,k-1})\big) \end{aligned}$$

for the 3d Poisson equation $\Delta u=f$ is of fourth order.

Proof. Analogously to the proof of Proposition 4.1, the truncation error is

$$\tau_{i,j,k}=\frac{h^2}{12}(u_{xxxx}+u_{yyyy}+u_{zzzz})+O(h^4)$$

[1] In view of the large number of terms, the following Mathematica (Wolfram Research Inc.) code is useful to calculate all the $81+25$ terms in the discretization.

```
U[u_, i_, j_] := (1/6) ((u /. {i -> i + 1, j -> j + 1})
                      + (u /. {i -> i + 1, j -> j - 1})
                      + (u /. {i -> i - 1, j -> j + 1})
                      + (u /. {i -> i - 1, j -> j - 1}))
                + (2/3) ((u /. {i -> i + 1}) + (u /. {i -> i - 1})
                      + (u /. {j -> j + 1}) + (u /. {j -> j - 1}))
                - (10/3) u
Expand[U[U[u[i, j, k, l], i, j], k, l]]

F[f_, i_, j_] := (1/12) ((f /. {i -> i + 1}) + (f /. {i -> i - 1})
                       + (f /. {j -> j + 1}) + (f /. {j -> j - 1}))
                + (2/3) f
Expand[F[F[f[i, j, k, l], i, j], k, l]]
```

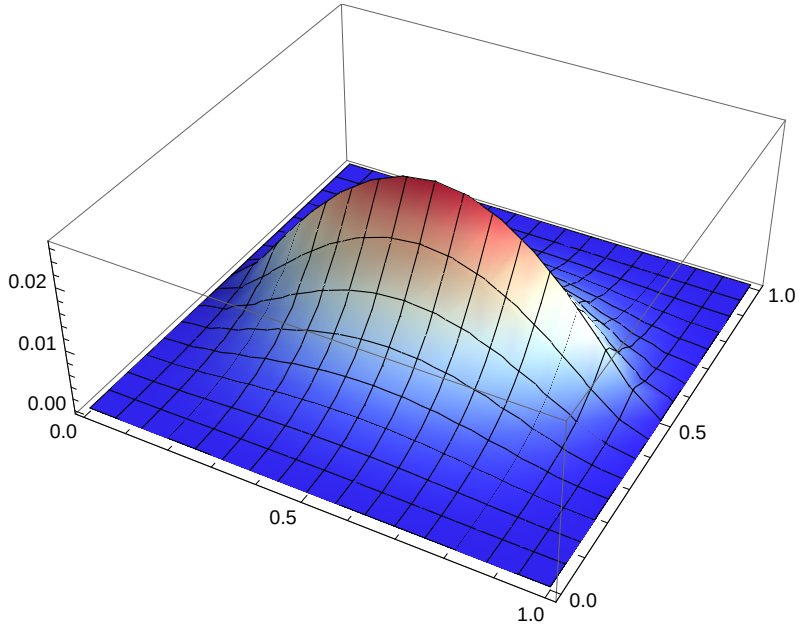

FIG. 4.1. *The variance as the diagonal $u(y_1,y_2,y_1,y_2)$ of the solution of $\Delta_y\Delta_z u(y_1,y_2,z_1,z_2)=\delta(y_1-\frac{1}{2})\delta(z_1-\frac{1}{2})$ on the domain $(0,1)^4$. This corresponds to $\bar{R}(y_2,y_3)=1$ in (3.5a).*

and we have

$$\begin{aligned} u_{xxxx} &= f_{xx} - u_{xxyy} - u_{xxzz}, \\ u_{yyyy} &= f_{yy} - u_{xxyy} - u_{yyzz}, \\ u_{zzzz} &= f_{zz} - u_{xxzz} - u_{yyzz}. \end{aligned}$$

This yields

$$\tau_{i,j,k} = \frac{h^2}{12}(f_{xx}+f_{yy}+f_{zz}) - \frac{h^2}{6}(u_{xxyy}+u_{xxzz}+u_{yyzz}) + O(h^4),$$

and the discretization

$$\begin{aligned} D_x^2 u_{i,j,k} + D_y^2 u_{i,j,k} + D_z^2 u_{i,j,k} + \frac{h^2}{6}(D_x^2 D_y^2 + D_x^2 D_z^2 + D_y^2 D_z^2) u_{i,j,k} \\ = f_{i,j,k} + \frac{h^2}{12}(D_x^2 + D_y^2 + D_z^2) f_{i,j,k} + O(h^4) \end{aligned}$$

is of fourth order. □

4.2. Numerical verification of the rate

To verify the homogenization result in Theorem 3.3 and the rate in Corollary 3.4, Monte-Carlo calculations are discussed in the following.

We consider a three-dimensional example for Corollary 3.4 with the scaling (3.15) in Corollary 3.4. We set $U := (0,1)^3 \subset \mathbb{R}^3$, define $L := -\Delta$, and use an equidistant grid for the finite-difference discretization of L. For symmetry, the boundary layer is located at $x = \frac{1}{2}$ so that the cells are

$$\mathcal{C}_k = \mathcal{C}_{(k_2,k_3)} = [\epsilon k_2, \epsilon(k_2+1)) \times [\epsilon k_3, \epsilon(k_3+1)).$$

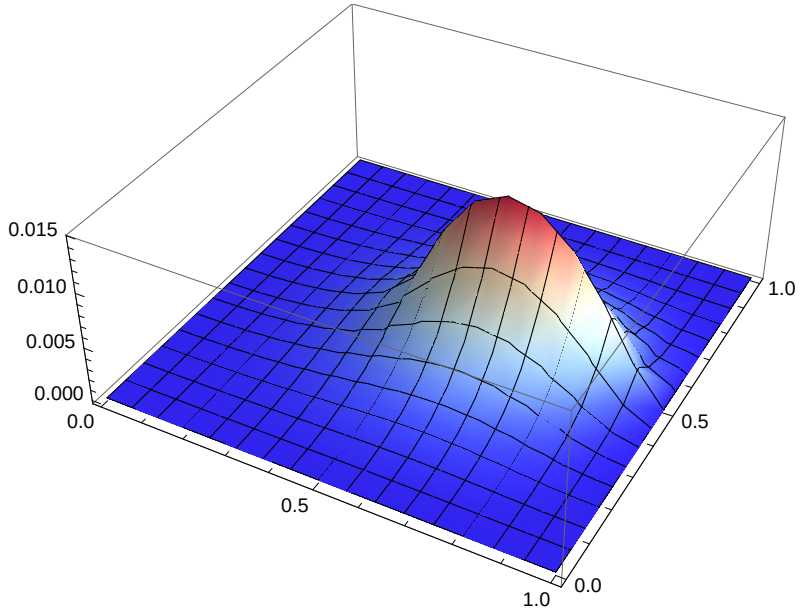

FIG. 4.2. *The variance as the diagonal* $u(y_1,y_2,y_1,y_2)$ *of the solution of* $\Delta_y\Delta_z u(y_1,y_2,z_1,z_2) = \delta(y_1-\frac{1}{2})\delta(z_1-\frac{1}{2})[y_2\geq\frac{1}{2}][z_2\geq\frac{1}{2}]$ *on the domain* $(0,1)^4$. *Here* $[y_2\geq\frac{1}{2}]$ *is the characteristic function of the set where* $y_2\geq\frac{1}{2}$ *holds true. This corresponds to* $\bar{R}(y_2,y_3)=[y_2\geq\frac{1}{2}][z_2\geq\frac{1}{2}]$ *in (3.5a).*

The number of cells in each direction in this example is chosen as $K_2 = K_3$ and as a power of two. In order to decrease the influence of the Dirichlet boundary conditions on the shape of the solution and hence to accelerate the calculation of the rate, mixed Dirichlet and Neumann boundary conditions are used: The boundary conditions are zero Dirichlet boundary conditions at $x_1 = 0$ and $x_1 = 1$ and zero Neumann boundary conditions at $x_2 = 0$, $x_2 = 1$, $x_3 = 0$, and $x_3 = 1$. The charge concentrations $\rho(x,\omega)$ are constant and uniformly distributed in the interval $[0,1]$ in each cell of the boundary layer.

The numerical verification for a large number of cells in the boundary layer is hampered by the fact that the direct or Monte-Carlo calculation of the variance requires many solutions of $Lu(x,\omega) = \rho(x,\omega)$ for randomly chosen ω. Calculations for total numbers of cells $K \in \{2^2,4^2,8^2,16^2\}$ were performed with a grid size of $1/16$ in the finite-difference approximation. To calculate the variance, 8192 realizations were used in all four cases.

To verify that the number of realizations is sufficient for the calculation of the variance, the integral of the variance over the domain U is shown as a function of the number of realizations in Fig. 4.3 for the case $K = 16^2$. Fig. 4.4 shows plots of the variances for $K \in \{2^2,4^2,8^2,16^2\}$ after 8192 realizations as the cell size is halved.

The results of the numerical calculations for the parameters described above are summarized in Table 4.1. As the number of cells in each direction is doubled in every refinement step, i.e., ϵ is halved, the scaling factor for the variance is given by Corollary 3.4 as $1/16$. The numerically approximated values of 7.8, 13.3, and 14.0 in

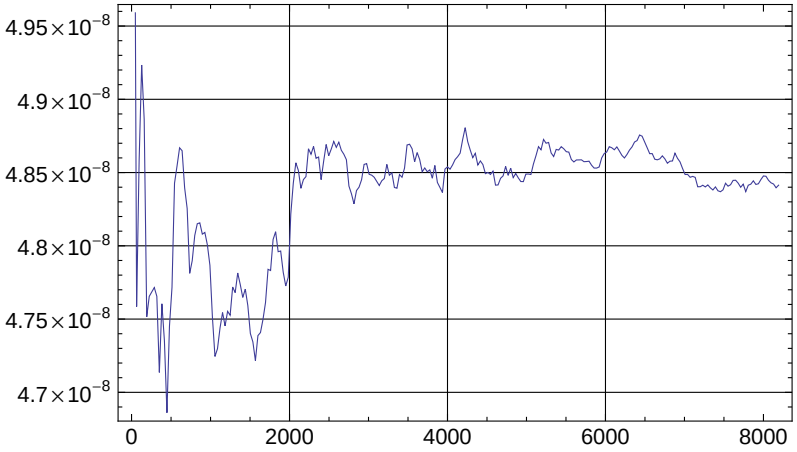

FIG. 4.3. *The integral* $\int_U \mathrm{var}\, u \mathrm{d}x$ *of the variance as a function of the number of realizations in a Monte-Carlo calculation for the case* $K = 16^2$.

ϵ	number of cells in boundary layer	integral of variance	scaling factor for variance
1/2	$K = 2^2$	$\int \mathrm{var}\, u = 7.0553 \cdot 10^{-5}$	
			7.8
1/4	$K = 4^2$	$\int \mathrm{var}\, u = 9.0360 \cdot 10^{-6}$	
			13.3
1/8	$K = 8^2$	$\int \mathrm{var}\, u = 6.7742 \cdot 10^{-7}$	
			14.0
1/16	$K = 16^2$	$\int \mathrm{var}\, u = 4.8414 \cdot 10^{-8}$	

TABLE 4.1. *Overview of the factors in the numerical verification. The predicted scaling factor for the variance is 16.*

Table 4.1 agree well with the theoretical value even for these small numbers of cells. The computational requirements for larger numbers of cells would be enormous due to the stochastic nature of the problem, which underlines the importance of the rate in Corollary 3.4.

5. Conclusion

In this work, we have treated the homogenization of boundary layers in stochastic elliptic partial differential equations. The main result is a limiting problems for the covariance of the solution of the stochastic equation. We have also deduced a rate for the covariance from the limiting problem. An existence and uniqueness result and further properties of the limiting equation for the covariance have also been shown. The numerical approximation of solutions of the covariance equation have also been discussed. Applications of this work include the simulation of electrostatics in nanotechnological devices such as field-effect sensors [18].

6. Acknowledgment

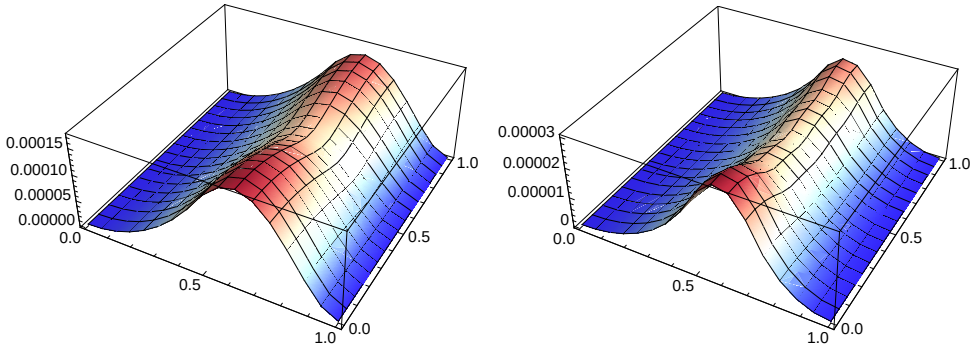

(a) $K=2^2$. (b) $K=4^2$.

(c) $K=8^2$. (d) $K=16^2$.

FIG. 4.4. *The variances after 8192 realizations for the four cases* $K\in\{2^2,4^2,8^2,16^2\}$. *The plots are two-dimensional ones for* $z=\frac{1}{2}$.

The authors acknowledge fruitful discussions with Robert W. Dutton and Yang Liu.

This work was supported by the FWF (Austrian Science Fund) project No. P20871-N13 and by the WWTF (Viennese Science and Technology Fund) project No. MA09-028. This publication is based on work supported by Award No. KUK-I1-007-43, funded by the King Abdullah University of Science and Technology (KAUST). This work was supported by the NSF under grants DMS-0604986 and DMS-0757309.

REFERENCES

[1] I. Babuška and P. Chatzipantelidis, *On solving elliptic stochastic partial differential equations*, Comput. Methods Appl. Mech. Engrg., 191 (2002), pp. 4093–4122.

[2] I. Babuška, F. Nobile, and R. Tempone, *A stochastic collocation method for elliptic partial differential equations with random input data*, SIAM Rev., 52 (2010), pp. 317–355.

[3] I. Babuška, R. Tempone, and G. Zouraris, *Galerkin finite element approximations of stochastic elliptic partial differential equations*, SIAM J. Numer. Anal., 42 (2004), pp. 800–825.

[4] ———, *Solving elliptic boundary value problems with uncertain coefficients by the finite element method: the stochastic formulation*, Comput. Methods Appl. Mech. Engrg., 194 (2005), pp. 1251–1294.

[5] G. Bal, *Central limits and homogenization in random media*, Multiscale Model. Simul., 7

(2008), pp. 677–702.
[6] G. Bal, R. Ghanem, and I. Langmore, *Large deviation theory for a homogenized and "corrected" elliptic ODE*, J. Differential Equations, 251 (2011), pp. 1864–1902.
[7] G. Bal and W. Jing, *Corrector theory for elliptic equations in random media with singular Green's function. Application to random boundaries*, Commun. Math. Sci., 9 (2011), pp. 383–411.
[8] S. Baumgartner and C. Heitzinger, *Existence and local uniqueness for 3d self-consistent multiscale models for field-effect sensors*, Commun. Math. Sci., 10 (2012), pp. 693–716.
[9] ———, *A one-level FETI method for the drift-diffusion-Poisson system with discontinuities at an interface*, J. Comput. Phys., (2013), pp. 1–26. *Accepted for publication.*
[10] S. Baumgartner, C. Heitzinger, A. Vacic, and M. A. Reed, *Predictive simulations and optimization of nanowire field-effect PSA sensors including screening*, Nanotechnology, pp. 1–16. *In review.*
[11] S. Baumgartner, M. Vasicek, A. Bulyha, and C. Heitzinger, *Optimization of nanowire DNA sensor sensitivity using self-consistent simulation*, Nanotechnology, 22 (2011), pp. 425503/1–8.
[12] S. Baumgartner, M. Vasicek, and C. Heitzinger, *Analysis of field-effect biosensors using self-consistent 3D drift-diffusion and Monte-Carlo simulations*, Procedia Engineering, 25 (2011), pp. 407–410.
[13] ———, *Modeling and simulation of nanowire based field-effect biosensors*, in Chemical Sensors: Simulation and Modeling, G. Korotcenkov, ed., Momentum Press, 2012, pp. 447–469.
[14] A. Bulyha and C. Heitzinger, *An algorithm for three-dimensional Monte-Carlo simulation of charge distribution at biofunctionalized surfaces*, Nanoscale, 3 (2011), pp. 1608–1617.
[15] L. Caffarelli and P. Souganidis, *Rates of convergence for the homogenization of fully nonlinear uniformly elliptic PDE in random media*, Invent. Math., 180 (2010), pp. 301–360.
[16] L. Caffarelli, P. Souganidis, and L. Wang, *Homogenization of fully nonlinear, uniformly elliptic and parabolic partial differential equations in stationary ergodic media*, Comm. Pure Appl. Math., 58 (2005), pp. 319–361.
[17] M. Deb, I. Babuška, and J. Oden, *Solution of stochastic partial differential equations using Galerkin finite element techniques*, Comput. Methods Appl. Mech. Engrg., 190 (2001), pp. 6359–6372.
[18] C. Heitzinger, Y. Liu, N. Mauser, C. Ringhofer, and R. W. Dutton, *Calculation of fluctuations in boundary layers of nanowire field-effect biosensors*, J. Comput. Theor. Nanosci., 7 (2010), pp. 2574–2580.
[19] C. Heitzinger, N. Mauser, and C. Ringhofer, *Multiscale modeling of planar and nanowire field-effect biosensors*, SIAM J. Appl. Math., 70 (2010), pp. 1634–1654.
[20] C. Heitzinger and C. Ringhofer, *A transport equation for confined structures derived from the Boltzmann equation*, Commun. Math. Sci., 9 (2011), pp. 829–857.
[21] H. Holden, B. Øksendal, J. Ubøe, and T. Zhang, *Stochastic Partial Differential Equations*, Springer-Verlag, New York, Dordrecht, Heidelberg, London, 2nd ed., 2010.
[22] H. Huang, C. Ong, J. Guo, T. White, M. Tsea, and O. Tana, *Pt surface modification of SnO_2 nanorod arrays for CO and H_2 sensors*, Nanoscale, 2 (2010), pp. 1203–1207.
[23] A. Jentzen and P. Kloeden, *The numerical approximation of stochastic partial differential equations*, Milan J. Math., 77 (2009), pp. 205–244.
[24] A. Keese, *A review of recent developments in the numerical solution of stochastic partial differential equations (stochastic finite elements)*, Informatikbericht 2003-06, Institute of Scientific Computing, Technical University Braunschweig, Brunswick, Germany, Oct. 2003.
[25] A. Köck, A. Tischner, T. Maier, M. Kast, C. Edtmaier, C. Gspan, and G. Kothleitner, *Atmospheric pressure fabrication of SnO_2-nanowires for highly sensitive CO and CH_4 detection*, Sens. Actuators B, 138 (2009), pp. 160–167.
[26] G. D. Maso and L. Modica, *Nonlinear stochastic homogenization and ergodic theory*, J. Reine Angew. Math., 368 (1986), pp. 28–42.
[27] H. Matthies and A. Keese, *Galerkin methods for linear and nonlinear elliptic stochastic partial differential equations*, Comput. Methods Appl. Mech. Engrg., 194 (2005), pp. 1295–1331.
[28] M. Punzet, D. Baurecht, F. Varga, H. Karlic, and C. Heitzinger, *Determination of surface concentrations of individual molecule-layers used in nanoscale biosensors by in-situ ATR-FTIR spectroscopy*, Nanoscale, 4 (2012), pp. 2431–2438.
[29] S. Steinhauer, E. Brunet, T. Maier, G. Mutinati, A. Köck, W.-D. Schubert, C. Edtmaier, C. Gspan, and W. Grogger, *Synthesis of high-aspect-ratio CuO nanowires for conductometric gas sensing*, Procedia Engineering, 25 (2011), pp. 1477–1480.

[30] E. Stern, J. Klemic, D. Routenberg, P. Wyrembak, D. Turner-Evans, A. Hamilton, D. LaVan, T. Fahmy, and M. Reed, *Label-free immunodetection with CMOS-compatible semiconducting nanowires*, Nature, 445 (2007), pp. 519–522.

[31] E. Stern, A. Vacic, N. Rajan, J. Criscione, J. Park, B. Ilic, D. Mooney, M. Reed, and T. Fahmy, *Label-free biomarker detection from whole blood*, Nature Nanotechnology, 5 (2010), pp. 138–142.

[32] A. H. Talasaz, M. Nemat-Gorgani, Y. Liu, P. Ståhl, R. W. Dutton, M. Ronaghi, and R. W. Davis, *Prediction of protein orientation upon immobilization on biological and nonbiological surfaces*, Proc. Nat. Acad. Sci. U.S.A., 103 (2006), pp. 14773–14778.

[33] B. Tian, T. Cohen-Karni, Q. Qing, X. Duan, P. Xie, and C. Lieber, *Three-dimensional, flexible nanoscale field-effect transistors as localized bioprobes*, Science, 329 (2010), pp. 830–834.

[34] A. Tischner, T. Maier, C. Stepper, and A. Köck, *Ultrathin SnO_2 gas sensors fabricated by spray pyrolysis for the detection of humidity and carbon monoxide*, Sens. Actuators B, 134 (2008), pp. 796–802.

[35] X. Wan, B. Rozovskii, and G. Karniadakis, *A stochastic modeling methodology based on weighted Wiener chaos and Malliavin calculus*, Proc. Nat. Acad. Sci. U.S.A., 106 (2009), pp. 14189–14194.

[36] G. Zheng, F. Patolsky, Y. Cui, W. Wang, and C. Lieber, *Multiplexed electrical detection of cancer markers with nanowire sensor arrays*, Nature Biotechnology, 23 (2005), pp. 1294–1301.

[37] A. Zima, A. Köck, and T. Maier, *In- and Sb-doped tin oxide nanocrystalline films for selective gas sensing*, Microelectronic Engineering, 87 (2010), pp. 1467–1470.